

Interplay of hybrid and unhybrid quantum transport of interacting electron pairs through a short conduction channel

Danhong Huang¹, Godfrey Gumbs², Yonatan
Abranyos², Michael Pepper^{3,4} and Sanjeev Kumar^{3,4}

¹*Air Force Research Laboratory, Space Vehicles Directorate,
Kirtland Air Force Base, New Mexico 87117, USA*

²*Department of Physics and Astronomy,
Hunter College of the City University of New York,
695 Park Avenue, New York, New York 10065, USA*

³*Department of Electronic and Electrical Engineering,
University College London, London, WC1E 7JE, United Kingdom*

⁴*London Centre for Nanotechnology, 17-19 Gordon Street,
London, WC1H 0AH, United Kingdom*

(Dated: June 7, 2022)

Abstract

For quantum ballistic transport of electrons through a short conduction channel, the role of Coulomb interaction may significantly modify the energy levels of an electron pair at low temperatures as the channel becomes wide. In this regime, the Coulomb effect on the orbital triplet and singlet electron-pair state is calculated and found to lead to four split energy levels, including two hybrid and two unhybrid states. Moreover, due to the interplay of hybrid and unhybrid Coulomb interactions between two electrons, our calculations reveal that the ground pair-state will switch from one hybrid orbit-triplet state (strong confinement) to the unhybrid orbit-singlet state (intermediate confinement) as the channel width gradually increases and then back to the original hybrid orbit-triplet state (weak confinement), due to larger total spin of the orbit-singlet state, as the channel width becomes larger than a threshold value. This switching behavior leaves a footprint in the conductance as well as in the diffusion thermoelectric power of electrons. Here, the predicted reoccurrence of the hybrid orbit-triplet state (spin-0 state) as a ground state is shown to relate to the higher spin degeneracy of the spin-1 state as well as to the strong Coulomb repulsion in the central region of the channel, which separates two electrons away and pushes them to different channel edges. The conductance reoccurrence region expands from the weak to the intermediate confinement regime with increasing linear electron density.

I. INTRODUCTION

For many years now, there has been a concerted effort to understand the behavior of the conductance of quantum wires under variable conditions of disorder, wire width and temperature for diffusive electron transport (for example, see Refs. [1–8]). For pure narrow samples of quantum wires whose widths are a few nanometers, the conductance plateaus are obtained as integer multiples of $2e^2/h$. It turns out that since the kinetic energy dominates over the Coulomb interaction in the limit of strong confinement, the conductance plateaus at integer multiples of $2e^2/h$ may be adequately accounted for in pure samples with the use of a single-particle picture⁹. However, as the width of the wire is increased, the Coulomb interaction between electrons plays more and more of a role in determining the values of the conductance plateaus.

The structural transition in a quasi-one-dimensional quantum-wire system was numerically predicted¹⁰ as early as in 2004 with a rich phase diagram. Later, a theoretical model for a split Wigner crystal into two chains (zigzag crystal) was proposed¹¹ in 2007 (for a review, see Ref. [12]). The effects of different pairwise repulsive interactions¹³, tunnel coupling of two parabolic channels¹⁴, different profiles of the confining channel¹⁵, and even a quantum-ring structure¹⁶ or the the surface of a cylinder¹⁷, on the continuous structural transitions of a Wigner crystal were further studied. Similar structural transitions of a Wigner crystal to a zigzag crystal in an ion chain¹⁸ and in quantum wires controlled by an external gate¹⁹ were also explored. In addition, the spin Peierls quantum phase transition in cold Coulomb crystals of trapped ions²⁰, the spontaneous spin polarization due to the electron-electron interactions under a bias-field control^{21,22}, and the phase diagram of zigzag Wigner crystals with spin coupling for two-, three and four-particle ring exchange processes²³, as well as melting of a quasi-one-dimensional Wigner crystal observed from the nonlinear resistivity²⁴ of electrons confined in quasi-one dimensional channels formed on the surface of superfluid ⁴He, were reported.

Despite the extensive theoretical studies on zigzag crystals for a long quantum wire, however, in a recent experiment²⁵ for a short conduction channel formed by split gates, one finds that, as the top gate voltage is increased, the conductance for a wide wire at the interface of a GaAs/AlGaAs heterostructure jumps from zero to $4e^2/h$, bypassing the $2e^2/h$ plateau which is encountered for narrow wires. For the picture of splitting into two rows,

the evolution of the crossing or anti-crossing of energy levels is not fully understood, and the purpose of this paper is to provide a microscopic theory which explains this observed phenomenon.

Additionally, we predict that the competition between the kinetic, direct Coulomb and quantum mechanical exchange energy in wires of intermediate widths should lead to fundamental differences from that obtained in the two extreme limits of very narrow and very wide wires. We have demonstrated that these differences may be traced to the nature of the ground state as the wire width is varied.

In related work, there have been several physical properties of the measured conductance of quasi-one-dimensional quantum wires which have been attributed to scattering from disorder potentials, the formation of a quantum dot within the channel caused by the presence of an impurity, as well as imperfections in the device geometry.⁵ These imperfections may lead to deviations from integer multiples of $2e^2/h$ for the values of the conductance plateaus or resonance structure such as oscillations superimposed on the conductance trace.^{4,26} Electron tunneling through the quantum dot in the channel as well as interference effects due to electron back-scattering from an impurity potential are believed to be responsible for these deviations in the values of the conductance plateaus of narrow quantum wires.⁴

In chemistry, hybridization is the well-known concept for mixing atomic orbitals into new hybrid ones (with different energies, shapes, etc., than the component atomic orbitals), suitable for the pairing of electrons to form chemical bonds in valence bond theory. Electronic orbital hybridization discussed in this paper means the mixing of orbitals of two interacting electron pairs to form a new ground and excited paired states²⁵. The Coulomb interaction for electron pairs can be used for building up the hybrid states while the pair ballistically passes along a one-dimensional conduction channel. Our calculations reveal the role and the existence of these interacting hybrid states in quasi-one-dimensional quantum ballistic transports. More importantly, we demonstrate in our work that the degree and significance of hybridization (Coulomb-induced level anticrossing) within such a structure may be tuned independently by varying the channel confinement with the use of a top gate.

In this paper, we confine our attention to a quasi-one-dimensional quantum wire containing a low density of electrons. We concentrate our efforts on calculating the lowest eigenstates for a pair of interacting electrons since this sheds some light on the role played

by electron-electron interaction in determining the nature of the ground state of a dilute electron system and consequently the lowest quantum conductance. The complicated pair tunneling process^{27,28} will not be considered here since it does not lead to conductance plateaus observed in our experiment. We show below that there is a range of values of wire widths where the two-electron transport are hybrid by Coulomb interaction, and therefore, it is not possible to describe the conductance in terms of a single-particle picture.

II. MODEL

The eigenstates of a pair of interacting electrons under the influence of a harmonic confining potential have been evaluated by several authors.^{29,30} In the paper by Wagner, et al.,²⁹ a quantum dot with a symmetric harmonic oscillator potential to confine the electrons was considered and it was noted that, consistent with Kohn's theorem³⁰, the Coulomb interaction affects only the relative motion but not the center-of-mass properties. It was then demonstrated with the use of perturbation theory that as the strength of an external perpendicular magnetic field is increased, the ground state oscillates between a spin-singlet and a spin-triplet mode. Bryant³⁰ showed correlation effects between electrons depend on the size of the boxes containing them. By solving the Schrödinger equation exactly for a pair of interacting electrons, we demonstrate how correlations may determine the ground state and give rise to quasi-particles which participate in the transport processes.

If the scattering by either randomly distributed impurities and defects or by phonons are neglected at low temperatures for high-mobility short channel samples, the coherence in the wave functions of electron pairs may be maintained during pair transport along the channel. Additionally, if the transmission coefficient for the injection of electron pairs into the channel is close to unity in the absence of a significant reflection from potential barriers in their path and inelastic scattering between different pair states, we are able to use a quantum ballistic transport model for interacting electron pairs as far as the Coulomb interaction between electrons in the channel is fully taken into account. Our quantum ballistic system with transport of interacting electron pairs is shown schematically in Fig. 1.

For a fixed linear electron density n_{1D} , the pair chemical potential $\mu_p(T, n_{1D})$ within the channel can be determined from

$$n_{1D} = \frac{2}{\pi} \sum_{j=1}^4 \int_0^{\infty} dk_y \left\{ \exp \left[\frac{E_{j,k_y}^{(p)} - \mu_p}{k_B T} \right] + 1 \right\}^{-1}, \quad (1)$$

where k_y is the wave vector of electrons along the channel, T is the system temperature, $E_{j,k_y}^{(p)} = E_j^{(p)} + \hbar^2 k_y^2 / m^*$, labeled by (p) for $j = 1, 2, 3, 4$, represents the lowest four conduction energy subbands of an interacting electron pair, and m^* is the effective electron mass. In addition, the chemical potentials for the left and right electrodes are $\mu_L^{(p)}(V_b, T, n_{2D}) = \mu_p(T, n_{1D}) + eV_b$ and $\mu_R^{(p)}(V_b, T, n_{2D}) = \mu_p(T, n_{1D}) - eV_b$ in the presence of the low biased voltage V_b , where V_b is the applied biased voltage.

For quantum ballistic charge/heat transport of interacting electron pairs in the channel, the charge ($\alpha = 0$) and the heat ($\alpha = 1$) current densities are calculated according to⁹

$$J^{(\alpha)}(V_b, T, n_{1D}) = \frac{(-2e)^{1-\alpha}}{\pi} \sum_{j=1}^4 \int_0^{\infty} dk_y (E_{j,k_y}^{(p)} - \mu_p)^\alpha |v_{j,k_y}| \left[f_L(E_{j,k_y}^{(p)}) - f_R(E_{j,k_y}^{(p)}) \right], \quad (2)$$

where $v_{j,k_y} = \hbar k_y / m^*$ is the group velocity of an electron pair, $f_L(E_{j,k_y}^{(p)})$ and $f_R(E_{j,k_y}^{(p)})$ correspond to Fermi functions for noninteracting electron pairs in the left (L) and right (R) electrodes with associated chemical potentials $\mu_L^{(p)}$ and $\mu_R^{(p)}$ for noninteracting pairs, respectively.

For the interacting electron pair, its energy levels $E_j^{(p)} = E_{j,k_y=0}^{(p)}$, as shown in Fig. 2, are calculated as $E_1^{(p)} \equiv E_-^{(p)} = \varepsilon_0 + \varepsilon_1 + (u_{11} + u_{22})/2 - \Delta_C$, $E_2^{(p)} \equiv E_+^{(p)} = \varepsilon_0 + \varepsilon_1 + (u_{11} + u_{22})/2 + \Delta_C$, $E_3^{(p)} = \varepsilon_0 + \varepsilon_1 + u_{33}$ and $E_4^{(p)} = \varepsilon_0 + \varepsilon_1 + u_{44}$, where the Coulomb coupling term for the hybrid pair states is given by $\Delta_C = \sqrt{[\varepsilon_1 - \varepsilon_0 + (u_{22} - u_{11})/2]^2 + |u_{12}|^2}$. Here, the single-particle energy levels for harmonic-potential model with harmonic frequencies ω_x and ω_y in the transverse (x) and longitudinal (y) directions, respectively, are $\varepsilon_0 = (\hbar\omega_x + \hbar\omega_y)/2$ and $\varepsilon_1 = (3\hbar\omega_x + \hbar\omega_y)/2$, while the employed Coulomb interaction energies are found to be $u_{11} = N_0^2 E_c \mathcal{I}_{00,00}$, $u_{12} = N_0 N_1 E_c \mathcal{I}_{00,11}$, $u_{22} = N_1^2 E_c \mathcal{I}_{11,11}$, $u_{33} = N_0 N_1 E_c (\mathcal{I}_{01,01} + \mathcal{I}_{01,10})$ and $u_{44} = N_0 N_1 E_c (3\mathcal{I}_{01,01} - \mathcal{I}_{01,10})$, where $E_c = e^2 / 4\pi\epsilon_0\epsilon_r L_y$ in terms of the length L_y of the channel and the background dielectric constant ϵ_r , $N_n = \{\exp[(\varepsilon_n - \mu_0)/k_B T] + 1\}^{-1}$ ($n = 0, 1$) is the single-particle level occupation factor, and $\mu_0(T, n_{1D})$ is the single-electron chemical potential. Right before a pair of electrons is being injected into a conduction channel, these two electrons can select individual subband (same or different subbands and

lower or higher subbands) for their ballistic transport. Such a selection is subjected to subband population by the pool of electrons within the channel. Right after this pair of electrons are injected into the channel, they will interact to each other through either intrasubband or intersubband Coulomb coupling. The ballistic injection of electron pairs and the existence of an electron pool in the conduction channel are reflected in the inclusion of these two level occupation factors. The symbol $\mathcal{I}_{\alpha\beta,\gamma\delta}$ represents the Coulomb integral for $\alpha, \beta, \gamma, \delta = 0, 1$ if we only consider interacting pair states formed from the lowest ('0') and first excited ('1') state.

Finally, for the harmonic-potential model, the four dimensionless Coulomb integrals introduced above are calculated as

$$\begin{aligned}
\mathcal{I}_{00,00}(\mathcal{R}) &= \sqrt{\frac{2}{\pi}} \int_0^\pi \frac{d\theta}{[1 + (\mathcal{R}^2 - 1) \cos^2 \theta]^{1/2}}, \\
\mathcal{I}_{11,11}(\mathcal{R}) &= \sqrt{\frac{2}{\pi}} \int_0^\pi \frac{d\theta}{[1 + (\mathcal{R}^2 - 1) \cos^2 \theta]^{1/2}} \\
&\quad \times \left\{ 1 - \frac{\mathcal{R}^2 \cos^2 \theta}{1 + (\mathcal{R}^2 - 1) \cos^2 \theta} + \frac{3\mathcal{R}^4 \cos^4 \theta}{4[1 + (\mathcal{R}^2 - 1) \cos^2 \theta]^2} \right\}, \\
\mathcal{I}_{01,01}(\mathcal{R}) &= \frac{1}{\sqrt{2\pi}} \int_0^\pi d\theta \frac{2 + (\mathcal{R}^2 - 2) \cos^2 \theta}{[1 + (\mathcal{R}^2 - 1) \cos^2 \theta]^{3/2}}, \\
\mathcal{I}_{01,10}(\mathcal{R}) &= \frac{1}{\sqrt{2\pi}} \int_0^\pi d\theta \frac{\mathcal{R}^2 \cos^2 \theta}{[1 + (\mathcal{R}^2 - 1) \cos^2 \theta]^{3/2}}, \tag{3}
\end{aligned}$$

where the parameter $\mathcal{R} = W_x/L_y$ is the geometric ratio with W_x denoting the width of the conduction channel. For $\mathcal{R} \gg 1$, all the four terms in Eq. (3) scale as $1/\mathcal{R}$.

By using the calculated $J^{(\alpha)}(V_b, T, n_{1D})$ in Eq. (2), the electrical conductance $G(T, n_{1D})$ and the diffusion thermoelectric power $S_d(T, n_{1D})$ of an interacting electron pair can be expressed as⁹

$$\begin{aligned}
G(T, n_{1D}) &= \frac{J^{(\alpha=0)}(V_b, T, n_{1D})}{V_b}, \\
S_d(T, n_{1D}) &= \frac{1}{T} \frac{J^{(\alpha=1)}(V_b, T, n_{1D})}{J^{(\alpha=0)}(V_b, T, n_{1D})}. \tag{4}
\end{aligned}$$

In the next section, we present and discuss our numerical calculation and their relationship to the recently reported results in Ref. [25].

III. DISCUSSION

A. Theoretical Results

In all our numerical calculations, we set $T = 10$ mK, $V_b = 0.01$ mV, $L_y = 400$ nm, $\epsilon_r = 12$, and $m^*/m_0 = 0.067$ (with free-electron mass m_0). Here, the quantum ballistic transport of hybrid pairs of electrons through a conduction channel is defined as one moving through either one of orbit-triplet states $E_{\pm}^{(p)}$.

For an interacting (hybrid) electron pair, their energy levels $E_j^{(p)}$ are expected to depend on the electron density n_{1D} , as shown in Fig. 2. When the geometry ratio $\mathcal{R} = W_x/L_y$ is small for strong confinement in (a), only the ground state $E_-^{(p)}$ is affected by varying n_{1D} . As \mathcal{R} increases to 0.6 in (b), the level crossing between $E_-^{(p)}$ of the hybrid state and the degenerate $E_3^{(p)} = E_4^{(p)}$ of the unhybrid state, as well as level anticrossing between $E_-^{(p)}$ and $E_+^{(p)}$ of two hybrid states, occur at lower densities. When $\mathcal{R} > 1$, as displayed in (c) and (d), Coulomb interaction between electrons becomes significant. As a result, both $E_3^{(p)}$ and $E_4^{(p)}$ levels of two hybrid states are greatly pushed up at higher densities (i.e., $N_1 > 0$), leading to a recovery of the ground state to $E_-^{(p)}$. In addition, the $E_4^{(p)}$ level for the spin-1 state in (c) and (d) changes from the degenerate ground state at lower n_{1D} to the highest-energy state at higher n_{1D} . On the other hand, in the presence of a transverse magnetic field, the $E_3^{(p)}$ level for the spin-0 state decouples from the magnetic field, while the degenerated $E_4^{(p)}$ level for the spin-1 state will be split into three by the Zeeman effect, leading to new e^2/h and $3e^2/h$ conductance plateaus³¹.

Figure 3 presents a comparison of conductance G for both a non-interacting and an interacting electron pair in the range of $0.1 \leq \mathcal{R} \leq 1$. For very strong confinement in (a), the Coulomb interaction effect is negligible and a conductance $2e^2/h$ plateau is clearly seen. As \mathcal{R} increases to 0.4 in (b) and 0.6 in (c) for cases with strong confinement, G for a non-interacting electron pair remains largely unchanged. For an interacting electron pair, however, the conductance $2e^2/h$ plateau in (a) is completely destroyed by Coulomb interaction and accompanied by the occurrence of a new $4e^2/h$ plateau for G . This behavior agrees with the result of both a unhybrid level-crossing and a hybrid level anticrossing observed in Fig. 2(b). This new $4e^2/h$ conductance plateau is greatly perturbed at higher densities by a sharp spike and a follow-up deep dip to the lower $2e^2/h$ plateau as $\mathcal{R} = 1$ for

intermediate confinement in (d).

We present in Fig. 4 the evolution of the conductance plateau with increasing \mathcal{R} in the weak confinement regime. When $\mathcal{R} \geq 1.6$, conductance plateaus for the non-interacting electron pair are washed out in (b), (c) and (d) due to very small single-particle energy level separation in comparison with the thermal energy $k_B T$. It is also clear that the incomplete $4e^2/h$ conductance plateau in (a) for the interacting electron pair is completely destroyed in this regime. However, the recovery of the single-particle-like $2e^2/h$ plateau, as seen in Fig. 3(a), can be seen in this plot. Additionally, the $2e^2/h$ plateau further expands and extends to lower and lower electron densities as \mathcal{R} increases up to 2.0. This unique reoccurrence feature can be fully explained by the rising energy levels at higher densities due to relatively enhanced Coulomb repulsion as displayed in Figs. 2(c) and (d).

For clarity, we note that as a pair of electrons are injected into a conduction channel, they may select specific subbands for their transport ballistically. This selection rule is determined by the occupation factor of the electrons already within the channel. During the period of time that the two injected moving electrons are within the channel, they may interact with each other through either the intrasubband or the intersubband Coulomb coupling. We emphasize that the linear density of electrons confined within the channel may be held constant when the channel width is varied. For this to occur, the Fermi energy will adjust itself to accommodate all electrons and additional subbands are populated accompanied by reduced energy level separations. Specifically, the Fermi energy is actually reduced and the number of electrons in the channel is not changed at all. Furthermore, although the Fermi energy is reduced, the second level may still be populated due to reduced level separation to keep the number of electrons in the channel a constant. Clearly, enhancement of the Coulomb interaction is not solely determined by the electron density, since it also depends on how electrons are distributed. For the Coulomb effect on the states of the pair of electrons, the inclusion of a new populated pair state, with one electron in a lower energy level and the other electron in a higher level, will induce a new Coulomb effect on the pair states of electrons.

As the transverse confinement becomes weaker (or the \mathcal{R} value is increased), the kinetic part of the energy levels $E_j^{(p)}$ of a pair will drop as $1/\mathcal{R}^2$ for fixed L_y . Therefore, by increasing \mathcal{R} , the significance of Coulomb interaction, which scales as $1/\mathcal{R}$ as shown by Eq. (3), will

be relatively enhanced. In addition, the second energy level will be occupied by increasing \mathcal{R} for fixed electron density due to reduced level separation. Consequently, the additional Coulomb repulsion between two electrons on different energy levels is introduced. This effect is reflected in Figs. 5(b), (c) and (d) as pushing up the energy levels $E_-^{(p)}$ and $E_3^{(p)}$ (as $N_1 > 0$) in the region of $\mathcal{R} > 1$ when $n_{1D} \geq 0.2 \times 10^5 \text{ cm}^{-1}$. Furthermore, the existence of three-fold spin degeneracy in the $E_4^{(p)}$ level pushes itself above the $E_3^{(p)}$ level as the Coulomb interaction is enhanced for $\mathcal{R} > 1$. However, the $E_+^{(p)}$ electron pair state, associated with two excited-state electrons, is still dominated by the kinetic energy for the whole range of \mathcal{R} shown in this figure. As n_{1D} further increases, the Coulomb repulsion effect extends to the intermediate confinement regime in Fig. 5(d). As a whole, we find the ground state $E_-^{(p)}$ level in (a) for small values of \mathcal{R} and n_{1D} (where the kinetic energy of electrons is dominant) is fully recovered in (d) for large values of \mathcal{R} and n_{1D} (where the Coulomb energy is dominant). It is interesting to note that there exists an intermediate confinement regime ($\mathcal{R} \gtrsim 1$) between the strong (scaling as fast drop $1/\mathcal{R}^2$ for $\mathcal{R} < 1$) and weak (scaling as slow drop $1/\mathcal{R}$ for $\mathcal{R} \gg 1$) confinement regimes, where the Coulomb interaction between electrons can be relatively highlighted to give rise to pushing up of three energy levels and the recovery of the the ground state $E_-^{(p)}$ level simultaneously.

The ground-state recovery observed in Fig. 5 has a profound influence both on the distribution of conductance plateaus and on the interplay of the electron hybridization, as displayed in Fig. 6. When n_{1D} is very small, the Coulomb effect can be neglected. In this case, the $2e^2/h$ conductance plateau is observed for the interacting electron pair as shown in (a) for all values of \mathcal{R} . As n_{1D} is increased to $0.2 \times 10^5 \text{ cm}^{-1}$ in (b), the $2e^2/h$ plateau in (a) is destroyed except for its recovery close to $\mathcal{R} = 2.0$. If the value of n_{1D} is further increased as in (c) and (d), the new $4e^2/h$ conductance plateau shows up for the interacting electron pair, which corresponds to the population of the degenerated lowest energy levels $E_3^{(p)}$ and $E_4^{(p)}$ after their crossing another $E_-^{(p)}$ energy level. As \mathcal{R} further increases above one in the very-weak confinement regime, the ground-state recovery, as discussed in Figs. 5(c) and (d), enforces the reoccurrence of the $2e^2/h$ conductance plateau due to strong Coulomb repulsion between electrons.

In order to get a complete picture of the quantum ballistic transport of interacting pairs of electrons passing through a one-dimensional conduction channel, we present the contour

plots of conductance G and diffusion thermoelectric power of electrons S_d as functions of \mathcal{R} and n_{1D} in Fig. 7 for both non-interacting and interacting electron pairs as a comparison. By comparing (a) and (b) for G , we find that the Coulomb effect is most dominant in the upper right-hand corner region of (b) within a weak confinement regime and a relatively high electron density, where a gradual conductance is replaced by a $2e^2/h$ conductance plateau due to strong Coulomb repulsion between electrons. In addition, we also find another $4e^2/h$ conductance plateau in the lower-right corner region of (b) (which is separated by a spike in G from the upper-right corner region), where confinement is intermediate or stronger but the electron density is high. From the comparison of (c) and (d), we find that the Coulomb interaction suppresses S_d in the weak confinement region and with a relatively high electron density. Under very strong confinement, a downward step in S_d outside its suppression region is seen for interacting electron pairs. Moreover, the spike in G also has a visible feature reflected in S_d .

B. Experimental Verification

Two-terminal differential conductance measurements were performed using an excitation voltage of $10\ \mu\text{V}$ at 73 Hz using the Oxford Instruments cryofree dilution refrigerator, where the device was estimated to have an electron temperature of around 70 mK.

A top gated, split gate device provides additional confinement to the 1D electrons which enables varying the confinement from being very strong (zero top gate) to very weak (very negative top gate voltage). In the present work, top gate voltage, V_{tg} was varied from 0 (left) to $-2.2\ \text{V}$ (right) in the steps of 50 mV.

The device used in the present work was fabricated from a modulation doped GaAs/AlGaAs heterostructure grown using a molecular beam epitaxy (MBE), where a two-dimensional electron gas (2DEG) is formed 300 nm beneath the interface. Typical dimensions of the split gate device are: length 400 nm and width 700 nm. A top gate covers the entire split gate sandwiching a crossed-linked PMMA layer of thickness 200 nm. The 2DEG sits around 300 nm beneath the surface of the GaAs/AlGaAs heterostructure. The 2DEG mobilities and electron densities are $3.5\text{-}5.0 \times 10^6\ \text{cm}^2/\text{Vs}$ and $1.8\text{-}2.2 \times 10^{11}\ \text{cm}^{-2}$, respectively.

Figure 8 shows the differential conductance plot of the device as a function of split gate voltage for various top gate voltages. As shown in Fig. 8, when the confinement is weakened, the $2e^2/h$ conductance plateau weakens. On further weakening the confinement, the $2e^2/h$ plateau disappears and a direct jump in conductance to the $4e^2/h$ plateau occurs at $V_{\text{tg}} = -2.05$ V. Eventually the first plateau at $2e^2/h$ comes back on further weakening the confinement at $V_{\text{tg}} = -2.2$ V.

On the other hand, from our calculated results in Figs. 3 and 4, we see the occurrence of the $2e^2/h$ conductance plateau for small values of \mathcal{R} in the strong-confinement regime, the $4e^2/h$ conductance plateau for intermediate confinement, and the $2e^2/h$ conductance plateau in the weak-confinement regime preceded by a double-kink structure.

Therefore, we conclude from above that the experimental observations agree well with our theoretical prediction in this paper. Therefore, this experimentally observed feature for switching conductance plateau can be explained by the switching of the ground state from $E_-^{(p)}$ to degenerated $E_3^{(p)}$ and $E_4^{(p)}$ and back to $E_-^{(p)}$, which is reflected as an upward jump from $2e^2/h$ to $4e^2/h$ and followed by another downward jump from $4e^2/h$ back to $2e^2/h$ with increasing channel width.

IV. CONCLUDING REMARKS

The ballistic conductance for a quasi-one dimensional channel (quantum wire) has exhibited interesting behavior as functions of the electron density as well as the confinement. We theoretically demonstrated that the electron-electron interaction explicitly plays a crucial role in our calculations in a weak-confinement regime. We carried out an extensive calculation of the effect of confinement on the conductance and the associated dependence on the interplay of hybrid and unhybrid quantum transport of two electrons. As shown through our numerical calculations, depending on the confinement parameter the conductance manifests the signature of single particle or hybrid particles behavior. This dependence can be observed in the variation of the conductance from $2e^2/h$ (single-particle) to $4e^2/h$ (unhybrid interaction) and back to $2e^2/h$ (hybrid interaction) as a function of the width of the quantum wire. It is interesting to observe how many-body effects enter into the calculation

of the quantum ballistic conductance.

- ¹ W. Smith, W. K. Hew, K. J. Thomas, M. Pepper, I. Farrer, D. Anderson, G. A. C. Jones and D. A. Ritchie, *Phys. Rev. B* **80**, 041306 (2009).
- ² W. K. Hew, K. J. Thomas, M. Pepper, I. Farrer, D. Anderson, G. A. C. Jones and D. A. Ritchie, *Phys. Rev. Lett.* **102**, 056804 (2009).
- ³ W. K. Hew, K. J. Thomas, M. Pepper, I. Farrer, D. Anderson, G. A. C. Jones and D. A. Ritchie, *Phys. Rev. Lett.* **101**, 036801 (2008).
- ⁴ L. W. Smith, K. J. Thomas, M. Pepper, D. A. Ritchie, I. Farrer, J. P. Griffiths and G. A. C. Jones, *J. Phys.: Conf. Ser.* **376**, 012018 (2012).
- ⁵ K. J. Thomas, J. T. Nicholls, M. Y. Simmons, M. Pepper, D. R. Mace and D. A. Ritchie, *Phys. Rev. Lett.* **77**, 135 (1996).
- ⁶ S. K. Lyo and D. H. Huang, *Phys. Rev. B*, **64**, 115320 (2001).
- ⁷ S. K. Lyo and D. H. Huang, *Phys. Rev. B* **68**, 115317 (2003).
- ⁸ S. K. Lyo and D. H. Huang, *Phys. Rev. B* **73**, 205336 (2006).
- ⁹ S. K. Lyo and D. H. Huang, *J. Phys.: Condens. Matter* **16**, 3379 (2004).
- ¹⁰ G. Piacente, I. V. Schweigert, J. J. Betouras and F. M. Peeters, *Phys. Rev. B* **69**, 045324 (2004).
- ¹¹ J. S. Meyer, K. A. Matveev and A. I. Larkin, *Phys. Rev. Lett.* **98**, 126404 (2007).
- ¹² J. S. Meyer and K. A. Matveev, *J. Phys.: Condens. Matter* **21**, 023203 (2009).
- ¹³ G. Piacente, G. Q. Hai and F. M. Peeters, *Phys. Rev. B* **81**, 024108 (2010).
- ¹⁴ J. E. Galván-Moya, K. Nelissen and F. M. Peeters, *Phys. Rev. B* **86**, 184102 (2012).
- ¹⁵ J. E. Galván-Moya, V. R. Misko and F. M. Peeters, *Phys. Rev. B* **90**, 094111 (2014).
- ¹⁶ A. C. Mehta, C. J. Umrigar, J. S. Meyer and H. U. Baranger, *Phys. Rev. Lett.* **110**, 246802 (2013).
- ¹⁷ E. Welandar, I. I. Yakimenko and K.-F. Berggren, *Phys. Rev. B* **82**, 073307 (2010).
- ¹⁸ E. Shimshoni, G. Morigi and S. Fishman, *Phys. Rev. A* **83**, 032308 (2011).
- ¹⁹ T. Meng, M. Dixit, M. Garst and J. S. Meyer, *Phys. Rev. B* **83**, 125323 (2011).
- ²⁰ A. Bermudez and M. B. Plenio, *Phys. Rev. Lett.* **109**, 010501 (2012).
- ²¹ A. D. Klironomos, J. S. Meyer and K. A. Matveev, *Europhys. Lett.* **74**, 679 (2006).
- ²² H. Lind, I. I. Yakimenko and K.-F. Berggren, *Phys. Rev. B* **83**, 075308 (2011).

- ²³ A. D. Klironomos, J. S. Meyer, T. Hikihara and K. A. Matveev, Phys. Rev. B **76**, 075302 (2007).
- ²⁴ H. Ikegami, H. Akimoto and K. Kono, Phys. Rev. B **82**, 201104(R) (2010).
- ²⁵ S. Kumar, K. J. Thomas, L. W. Smith, M. Pepper, G. L. Creeth, I. Farrer, D. Ritchie, G. Jones and J. Griffiths, Phys. Rev. B **90**, 201304(R) (2014).
- ²⁶ G. Gumbs, A. Balassis, D. H. Huang, S. Ahmed and R. Brennan, J. Appl. Phys. **110**, 073709 (2011).
- ²⁷ J. Koch, M. E. Raikh and F. von Oppen, Phys. Rev. Lett. **96**, 056803 (2006).
- ²⁸ M. Leijnse M. R. Wegewijs and M. H. Hettler, Phys. Rev. Lett. **103**, 156803 (2009).
- ²⁹ M. Wagner, U. Merkt and A. V. Chaplik, Phys. Rev. B. **45**, 1951 (1991).
- ³⁰ G. W. Bryant, Phys. Rev. Lett. **59**, 1140 (1987).
- ³¹ G. Gumbs, A. Balassis, and D. H. Huang, S. Ahmed and R. Brennan, J. Appl. Phys. **110**, 073709 (2011).

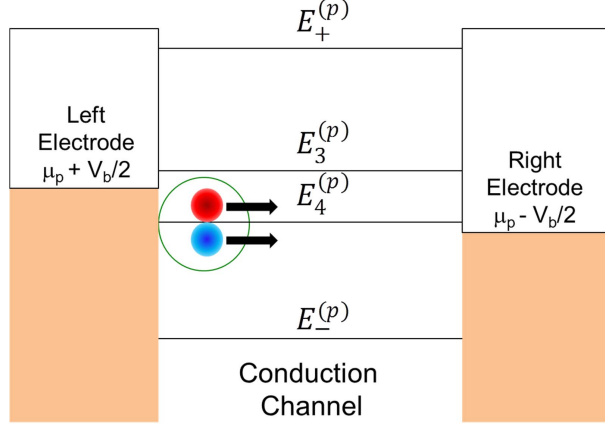


FIG. 1: (Color online) Schematic energy diagram of our model system, where an interacting electron pair is assumed to transport ballistically through a conduction channel, where the labels for different energy levels are explained in the text.

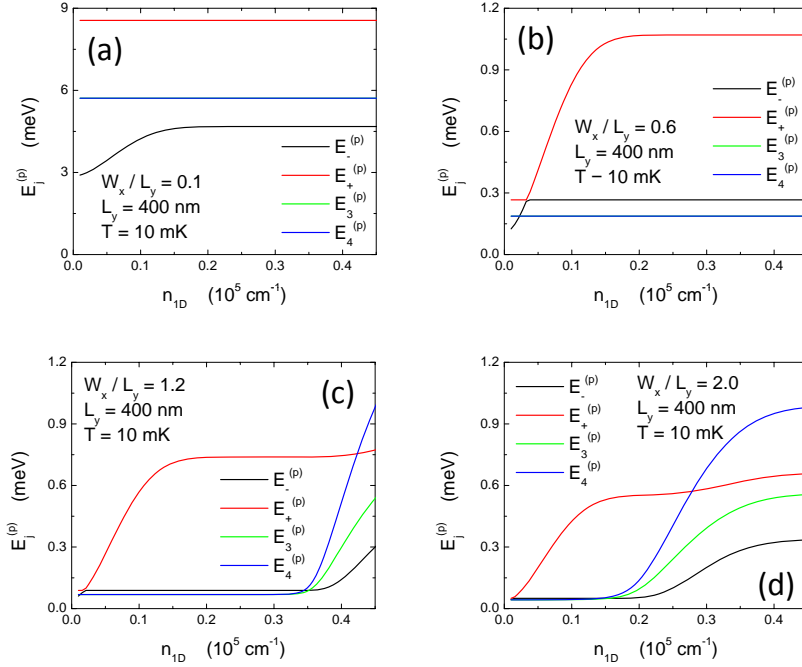


FIG. 2: (Color online) Plots of energy levels $E_j^{(p)}$ ($j = -, +, 3, 4$) of an interacting electron pair as a function of linear electron density n_{1D} with several values of $\mathcal{R} = W_x/L_y$. Here, we set $\mathcal{R} = 0.1$ (a), 0.6 (b), 1.2 (c) and 2.0 (d) for very strong to intermediate confinement.

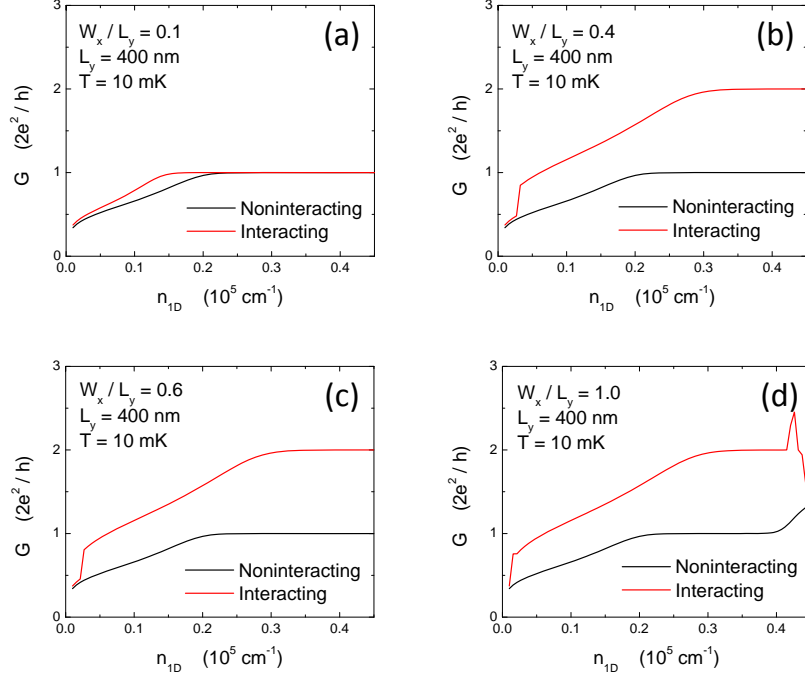


FIG. 3: (Color online) Plots of conductance G as a function of n_{1D} with several values of \mathcal{R} for both noninteracting (black curves) and interacting (red curves) cases. Here, we set $\mathcal{R} = 0.1$ (a), 0.4 (b), 0.6 (c) and 1.0 (d) for intermediate to weak confinement.

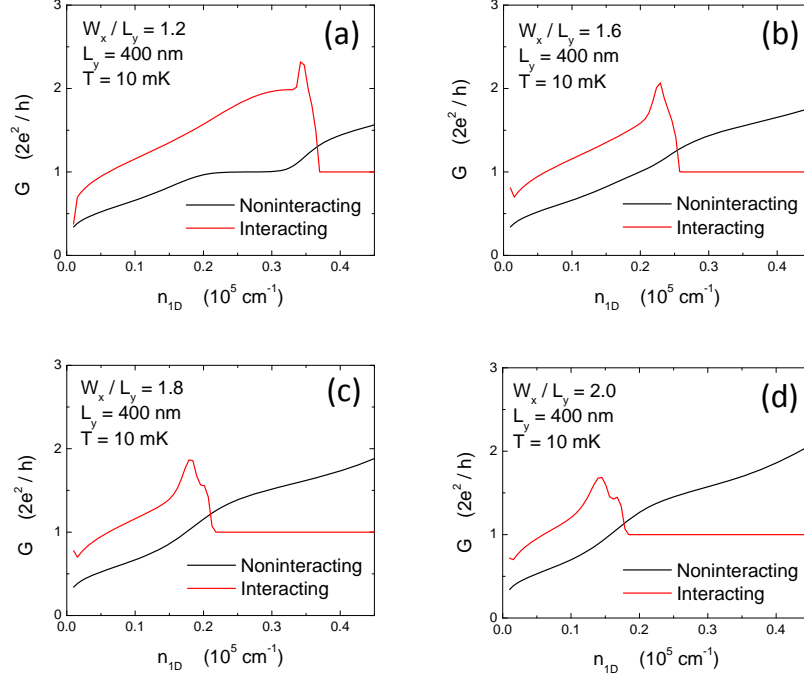


FIG. 4: (Color online) Plots of conductance G as a function of n_{1D} with several values of $\mathcal{R} = W_x/L_y$ for both noninteracting (black curves) and interacting (red curves) cases. Here, we set $\mathcal{R} = 1.2$ (a), 1.6 (b), 1.8 (c) and 2.0 (d).

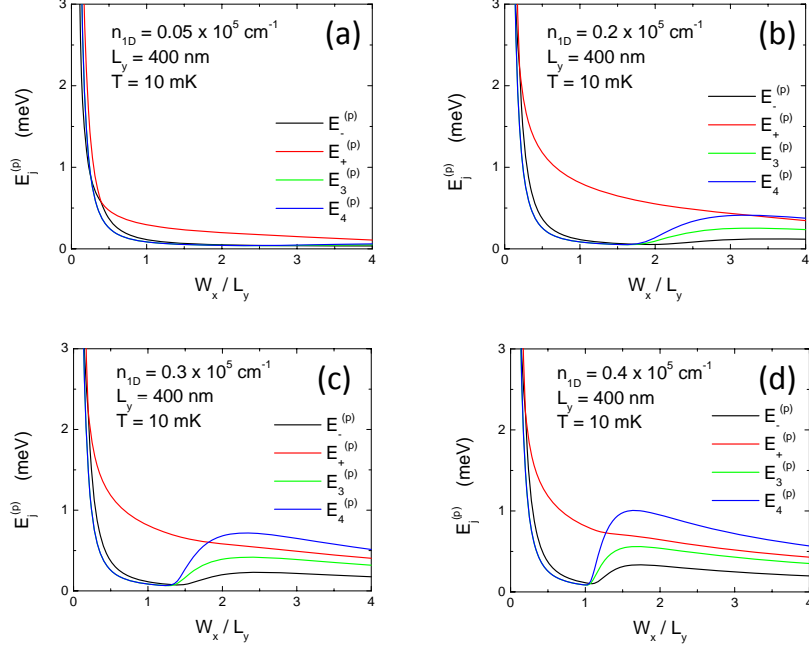


FIG. 5: (Color online) Plots of energy levels $E_j^{(p)}$ ($j = -, +, 3, 4$) of an interacting electron pair as a function of \mathcal{R} with several values of n_{1D} . Here, we set $n_{1D} = 0.05$ (a), 0.2 (b), 0.3 (c) and 0.4 (d) in unit of 10^5 cm^{-1} for increasing the significance of Coulomb interaction.

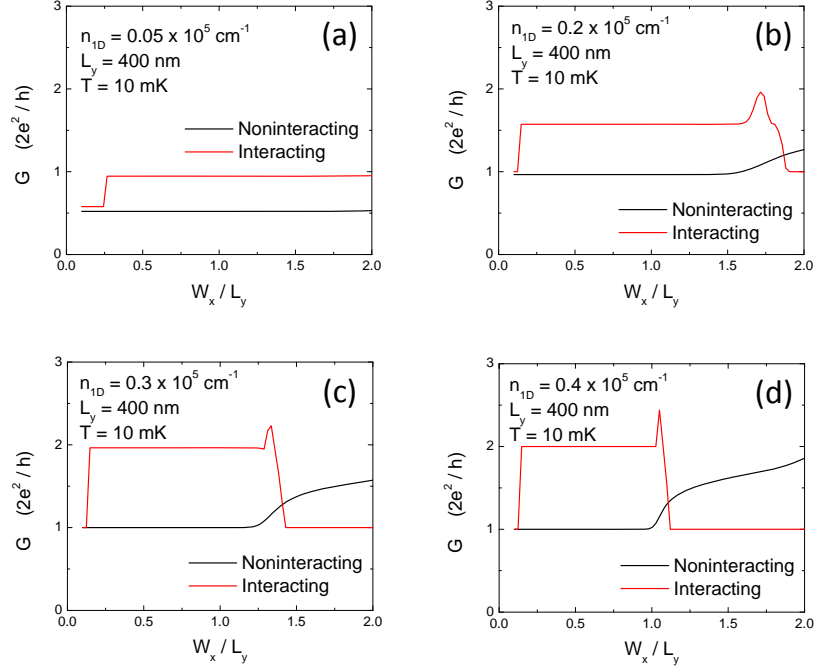


FIG. 6: (Color online) Plots of conductance G as a function of \mathcal{R} with several values of n_{1D} for both noninteracting (black curves) and interacting (red curves) cases. Here, we set $n_{1D} = 0.05$ (a), 0.2 (b), 0.3 (c) and 0.4 (d) in unit of 10^5 cm^{-1} .

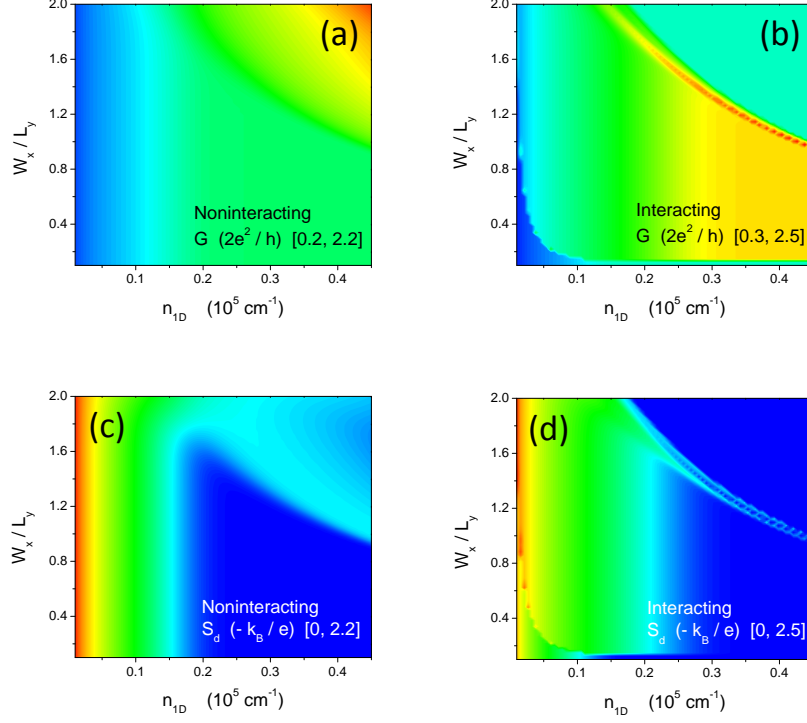


FIG. 7: (Color online) Contour plots of G [(a), (b)] and S_d [(c), (d)] as functions of both n_{1D} and \mathcal{R} for either noninteracting [(a), (c)] or interacting [(b), (d)] case.

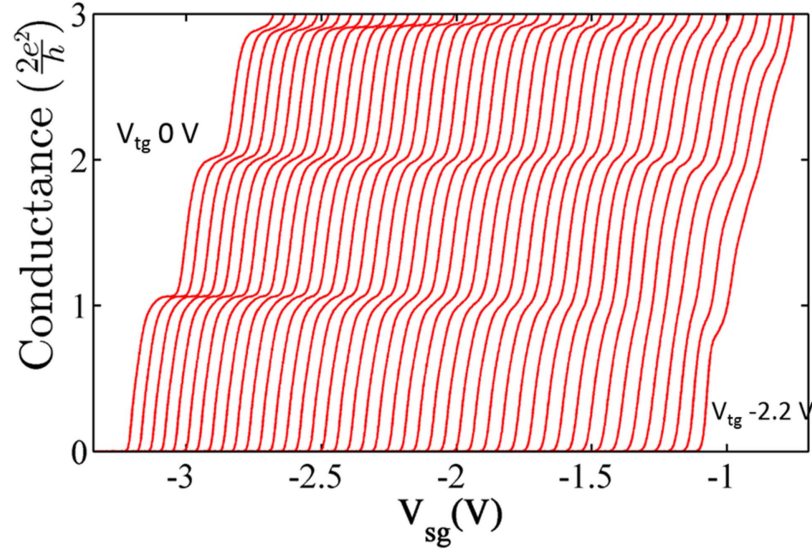


FIG. 8: (Color online) Plot for measured differential conductance, where a jump to $4e^2/h$ occurs when the confinement is weakened using a top gated, split-gate device. The confinement is controlled by making the top gate negative so that left(right) of the plot is strong(weak) confinement.